

Analytical derivation of DC SQUID response

I I Soloviev^{1,2,3}, N V Klenov^{1,3,4,5}, A E Schegolev⁴, S V Bakurskiy^{1,3} and M Yu Kupriyanov^{1,3,6}

¹Lomonosov Moscow State University Skobeltsyn Institute of Nuclear Physics, 119991, Moscow, Russia

²Lukin Scientific Research Institute of Physical Problems, Zelenograd, 124460, Moscow, Russia

³Moscow Institute of Physics and Technology, State University, Dolgoprudniy, Moscow region, Russia

⁴Physics Department, Moscow State University, 119991, Moscow, Russia

⁵N. L. Dukhov All-Russia Research Institute of Automatics, 127055, Moscow, Russia

⁶Solid State Physics Department, Kazan Federal University, 420008, Kazan, Russia

E-mail: isol@phys.msu.ru

Abstract. We consider voltage and current responses formation in DC SQUID with overdamped Josephson junctions in resistive and superconducting state in the frame of resistively shunted junction (RSJ) model. For simplicity we neglect the junction capacitance and the noise effect. Explicit expressions for the responses in resistive state were obtained for a SQUID which is symmetrical with respect to bias current injection point. Normalized SQUID inductance $l = 2eI_cL/\hbar$ (where I_c is the critical current of Josephson junction, L is the SQUID inductance, e is the electron charge and \hbar is the Planck constant) was assumed to be within the range $l \leq 1$, subsequently expanded up to $l \approx 7$ using two fitting parameters. SQUID current response in superconducting state was considered for arbitrary value of the inductance. Impact of small technological spread of parameters relevant for low-temperature superconductor (LTS) technology was studied with generalization of the developed analytical approach for a case of small difference of critical currents and shunt resistances of the Josephson junctions, and inequality of SQUID inductive shoulders for both resistive and superconducting states. Comparison with numerical calculation results shows that developed analytical expressions can be used in practical LTS SQUIDs and SQUID-based circuits design, e.g. large serial SQIF, drastically decreasing the time of simulation.

PACS numbers: 85.25.Dg, 85.25.Am

Keywords: DC SQUID, voltage response, current response, SQIF

1. Introduction

The superconducting quantum interference device (SQUID) is a basic component of superconductor electronics having numerous applications [1–3]. DC SQUID being basically a magnetic flux-to-voltage transformer is used e.g. in highly sensitive magnetometers [4–8], amplifiers [9–11], readout circuits [12] and antennas [13, 14]. These devices are routinely designed for fabrication process utilizing low-temperature superconductors (LTS) and tunnel Josephson junctions, which became a workhorse of modern superconducting electronics.

High accuracy of modern LTS fabrication technology allow for the construction of advanced SQUID-based structures with unconventional flux-to-voltage transformation. One example of such structures is Superconductor Quantum Array (SQA) [15] with highly linear voltage response. SQA can be based on superconducting quantum interference filters (SQIFs) resulting from SQUID arrays with unequal loops [16, 17], or bi-SQUID cells [18]. It was argued [19] that SQA can be a basis of active electrically small wideband superconductor antenna. Such antenna could provide significant advances to modern superconducting broadband radio-frequency receiving systems [20]. A variety of structures, like the ones mentioned above, were proposed and extensively studied both theoretically and experimentally in recent years [13–15, 18, 19, 21–29].

Qualitative understanding of SQUID or SQUID-based structure response [16–18, 29] can be based on analytical approach assuming the SQUID inductance to be approximately equal to zero [30, 31]. However, for quantitative estimation of designed LTS circuit characteristics, accounting for a certain real value of the inductance is inevitable.

Main effort in the development of time-averaged analytical dependencies for practical SQUID parameters was done during study of high-temperature superconductor (HTS) SQUIDs [32–37]. High noise level $\Gamma > 0.1$ ($\Gamma = 2\pi k_B T / I_c \Phi_0$, where k_B is the Boltzmann constant, I_c is the critical current of Josephson junction, $\Phi_0 = h/2e$ is the flux quantum, h is the Planck constant, e is the electron charge) and high value of SQUID inductance $L > 100$ pH are typical in this case, that results in $l\Gamma \geq 1$ ($l = 2\pi L I_c / \Phi_0$). Developed analytical approaches are valid for $l\Gamma \geq 1$ and based on solution of two-dimensional Fokker-Planck equation [32, 35]. Obtained expression for the voltage-flux func-

tion $\bar{v}(\phi_e)$ of symmetrical SQUID (where \bar{v} is the average voltage across the SQUID, and $\phi_e = \pi \Phi_e / \Phi_0$, Φ_e is the external magnetic flux) in the frame of these approaches is a simple harmonic function $\bar{v} = a \cos \phi_e + b$ (where a, b are constants), which is not intended for accurate description of the response shape. These methods are used mostly for estimation of the voltage response amplitude and corresponding maximum value of the transfer function. Analysis of the presented results done in Ref. [35] shows that the approaches can't be applied for LTS SQUIDs.

Perturbation analysis developed in the limit of small SQUID inductance l was shown to be well suited for study of some aspects of SQUID dynamics and characteristics like thermal escape problem [38], Shapiro steps [39], persistent current and magnetic susceptibility [40]. Though, study of time-averaged response for practical inductance values still requires numerical calculations [41].

It is interesting to note that an attempt to average SQUID voltage dynamics in the frame of another analytical approach, which is somewhat similar to the perturbation analysis, was undertaken even before the works [32, 35] on HTS SQUIDs. In 1983 Peterson and McDonald proposed their voltage and current expressions for DC SQUID with small but finite inductance [42]. In their method the SQUID difference phase $\psi = (\phi_1 - \phi_2)/2$ ($\phi_{1,2}$ are the Josephson phases of the first and the second junction) was expressed as a sum of the normalized external magnetic flux ϕ_e and a small correction x , which vanishes with the inductance, $\psi = -\phi_e + x$. The correction x was sought in a form of Fourier series, and so all final analytical expressions also contain a sum of certain series. This complexity complicates analysis of obtained solutions and their adaptation for more complex practical SQUID-based circuits like a bi-SQUID or a SQIF.

Despite of the fact that half a century is gone since the year of the first demonstration of quantum interference between two Josephson junctions connected in parallel by superconducting inductance [43], a shape of DC SQUID response still was not found analytically for practical parameters of the device at low temperature ($T \approx 4.2$ K). This statement is confirmed by the fact that practical circuit optimization is always performed in the frame of numerical analysis [19, 22, 23, 25, 28, 29] that slows down the design process.

Purpose of this paper is resolution of this long

standing problem with presentation of analytical analysis of DC SQUID voltage and current responses on applied magnetic flux in resistive state (see Section 2 and Section 3 correspondingly), and analysis of the current response in superconducting state (Section 3). The analysis includes consideration of effect of small technological spread of SQUID parameters relevant for LTS technology, which is presented in Section 4. While superconducting state is considered for arbitrary value of the inductance, resistive state is considered first for $l \leq 1$. Analytical voltage-flux and current-flux functions in resistive state for practical inductances up to $l \approx 7$ are obtained by fitting of numerical data in Section 5. We conclude the paper by discussion of applicability of the obtained analytical expressions to optimization of practical SQUID-based structures like SQIF. For simplicity we don't account for thermal noise and neglect capacitance of the Josephson junctions. Their effects on the responses of LTS DC SQUID with overdamped junctions having relatively high critical currents ($\Gamma \leq 10^{-3}$) are assumed to be small.

2. SQUID voltage

In this Section we consider the voltage response of symmetrical DC SQUID with inductance $l \leq 1$ (Fig. 1). In the frame of resistively shunted junction (RSJ) model [44] for overdamped Josephson junctions one can write simple equations for the currents $i_{1,2}$ flowing through the SQUID

$$i_{1,2} = \sin \phi_{1,2} + \dot{\phi}_{1,2},$$

where the currents are normalized to the critical current I_c and dot denotes time differentiation with normalized time $\tau = t\omega_c$, $\omega_c = 2\pi I_c R_n / \Phi_0$ is the characteristic frequency, and R_n is the shunt resistance of the junctions. Kirchoff equations for the SQUID produce the following system of differential equations:

$$\frac{l}{2} \dot{\psi} = -(\psi + \phi_e) - \frac{l}{2} \sin \psi \cos \theta, \quad (1a)$$

$$\dot{\theta} = \frac{i_b}{2} - \cos \psi \sin \theta, \quad (1b)$$

where $\theta = (\phi_1 + \phi_2)/2$ is the sum phase, $i_b = I_b/I_c$, $I_b \geq 0$ is the bias current.

Since the inductance is present only in equation (1a), we assume that it primarily affects the difference phase. Following works [18, 42] we consider the difference phase as a sum of slow-varying ψ_- and oscillating ψ_\sim parts. The last one is assumed to be small $\psi_\sim \ll 1$ for shunted junctions and the inductance value $l \leq 1$. SQUID voltage response $\bar{v} = w_J$ normalized to $I_c R_n$ product (where w_J is the Josephson frequency) is found in the following

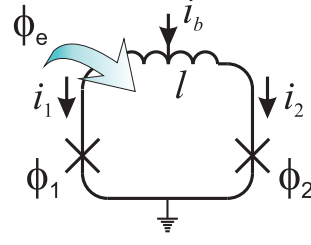


Figure 1. Symmetrical DC SQUID fed by bias current i_b and applied magnetic flux ϕ_e .

sequence. First, we obtain the solution $w_{J-} = \bar{\theta}$ assuming that $\psi = \psi_-$. Then we find ψ_\sim from (1a) using the determined θ , that in turn allows us to find the correction $w_{J\sim}$ and the total Josephson frequency $w_J = w_{J-} + w_{J\sim}$.

2.1. Solution for $\psi = \psi_-$

The difference phase is equal to it's slow-varying part in the limit of vanishing inductance $l \rightarrow 0$. Equation (1a) in this case gives $\psi = \psi_- = -\phi_e$, and an according solution of equation (1b) is well known (see Ref. [42] and references therein):

$$\tan \frac{\theta}{2} = z + \sqrt{1 - z^2} \tan \frac{i_b \sqrt{1 - z^2} \tau}{2}, \quad (2)$$

where $z = (2/i_b) \cos \phi_e$. The Josephson oscillation frequency can be obtained from (2) directly

$$w_{J-} = \frac{i_b}{2} \sqrt{1 - z^2} = \sqrt{\frac{i_b^2}{4} - \cos^2 \phi_e}. \quad (3)$$

It is worth to mention the known consistency of the expression (3) with the one for a single junction $w_J = \sqrt{i_b^2 - i_c^2}$, so one can treat $\cos \phi_e$ as an effective critical current and $i_b/2$ as an effective bias current. w_{J-} should be put zero if $i_b/2 < |\cos \phi_e|$.

2.2. Solution for $\psi = \psi_- + \psi_\sim$

Substitution of the difference phase as the sum $\psi_- + \psi_\sim$ into (1a) in the limit $\psi_\sim \ll 1$ converts this equation into

$$\frac{l}{2} \dot{\psi}_\sim = -\psi_\sim - \frac{l}{2} (\sin \psi_- + \psi_\sim \cos \psi_-) \cos \theta. \quad (4)$$

Solution of equation (4) has a form

$$\psi_\sim = \frac{l \sin \psi_- [l (\cos \psi_- - \frac{i_b}{2} \sin \theta) - 2 \cos \theta]}{l^2 w_{J-}^2 + 4}. \quad (5)$$

Its substitution into (1b) leads to correction of the Josephson frequency

$$w_J = \frac{i_b}{2} - \cos \psi_- \overline{\sin \theta} + \sin \psi_- \overline{\psi_\sim \sin \theta}. \quad (6)$$

Explicit form for w_J can be found by time averaging

$$w_J = w_{J-} - \frac{l^2 w_{J-}^2}{l^2 w_{J-}^2 + 4} \left(\frac{i_b}{2} - w_{J-} \right) \tan^2 \psi_-. \quad (7)$$

This expression describes SQUID voltage response for $l \leq 1$.

First factor of the second term in (7) suggests that decrease of the voltage response comes from filtering properties of the SQUID. This can be understood qualitatively on example of synchronization of the junctions by circulating current at external flux equal to half flux quantum $\phi_e = \pi/2$.

In general, the circulating current is defined as $i_{cir} = (i_1 - i_2)/2$. According to (1a) in resistive state it is $i_{cir} = -2\psi_-/l$ and with expression (5) it results to

$$i_{cir} = \frac{4\sqrt{1 + \frac{l^2 i_b^2}{16}}}{l^2 w_{J-}^2 + 4} \sin \psi_- \sin \left(\theta + \arctan \left[\frac{4}{li_b} \right] \right) - \frac{l \sin 2\psi_-}{l^2 w_{J-}^2 + 4}. \quad (8)$$

For the considered applied flux $\psi_- = -\phi_e = -\pi/2$ the sum phase is $\theta = w_{J-}\tau$ and the frequency $w_{J-} = i_b/2$ as it follows from (2), (3). Assuming that $l \ll 1$ the circulating current can be presented as $i_{cir} \approx -\cos(i_b\tau/2)$. This means that the total current through each junction in this case is

$$i_{1,2} = i_b/2 \mp \cos \left(\frac{i_b}{2} \tau \right). \quad (9)$$

Oscillating part of this current induces Shapiro steps in current-voltage (IV) curve of the junctions, see Fig. 2(a). Total width of the first step is [31] $2J_1(i_{cir}^a/w_{J-})$ (where $i_{cir}^a = 1$ is the amplitude of the circulating current in the limit $l \rightarrow 0$). Since the middle point of the step lies approximately at IV-curve of individual junction, the step starts with the current $\sqrt{(i_b/2)^2 + 1} - J_1(2/i_b) \approx i_b/2$ that is approximately equal to constant current applied to each junction.

Considering an increase of the inductance we note that the junctions are synchronized in antiphase at $\phi_e = \pi/2$. Thus the SQUID can be approximately analyzed as linear circuit presented in Fig. 2(b), which is a serial connection of two voltage generators and two resistors corresponding to two Josephson junctions, and inductance which couples them. From expression (9) we deduce that each generator provides harmonic voltage with normalized amplitude equal to unity. Amplitude of the current in such circuit is completely coincides with the amplitude of the considered circulating current (8)

$$i_{cir}^a = \frac{1}{\sqrt{1 + \frac{l^2 w_{J-}^2}{4}}}. \quad (10)$$

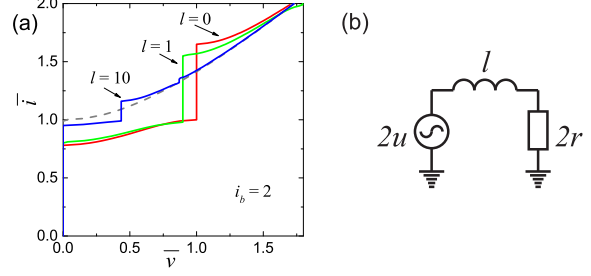


Figure 2. (a) IV curves of Josephson junction biased by current $i_b = i + i_{cir}^a \cos(w_J\tau)$, where i_{cir}^a corresponds to the amplitude of the circulating current and w_J corresponds to the Josephson frequency of a junction in the SQUID biased at $\phi_e = \pi/2$. The parameters i_{cir}^a , w_J are calculated for $i_b/2 = 1$ by expressions (10), (12) for $l = 0, 1$, and calculated numerically using (1) for $l = 10$. Dashed line corresponds to $i_{cir}^a = 0$. The IV curves are calculated numerically using (1). (b) LR-filter circuit used to analyze the SQUID at $\phi_e = \pi/2$.

Decrease of the amplitude of the oscillating current flowing through each junction with increase of the inductance leads to decrease of the first Shapiro step width. For fixed constant bias current this, in turn, leads to decrease of the oscillation frequency that shifts the Shapiro step, leading to synchronization of the junctions at lower frequency, see Fig. 2(a). This means that the decrease of the time-averaged SQUID voltage is caused by filtering of the circulating current, and the junctions are switched at frequency allowed by LR-relaxation time of the circuit.

Returning to expression (7) we note that at the point $\phi_e = \pi/2$ where $\tan^2 \psi_-$ is infinite the finite value of w_J can be found through the limit for the last two factors of the second term

$$\lim_{\phi_e \rightarrow \pi/2} \left(\frac{i_b}{2} - \sqrt{\frac{i_b^2}{4} - \cos^2 \phi_e} \right) \tan^2 \phi_e \rightarrow \frac{1}{i_b}. \quad (11)$$

Since $w_{J-}(\pi/2) = i_b/2$, the Josephson oscillation frequency at this point is

$$w_J(\pi/2) = \frac{i_b}{2} \left[1 - \frac{2l^2}{l^2 i_b^2 + 16} \right]. \quad (12)$$

This gives the amplitude of the voltage response $v_{pp} = w_J(\pi/2) - w_J(0)$

$$v_{pp} = \frac{i_b}{2} \left[1 - \frac{2l^2}{l^2 i_b^2 + 16} \right] - \sqrt{\frac{i_b^2}{4} - 1}, \quad (13)$$

where the last term should be put zero, if $i_b/2 < 1$.

It is seen that with the bias current increase both frequencies $w_J(\pi/2)$, $w_J(0)$ tend to $i_b/2$. Since the voltage response appears due to excitation of the circulating current, it vanishes in this case because circulating current portion in the total current flowing through the junctions becomes small. Since junctions in this limit are biased high above their critical current, time-averaged voltage on the SQUID corresponds to

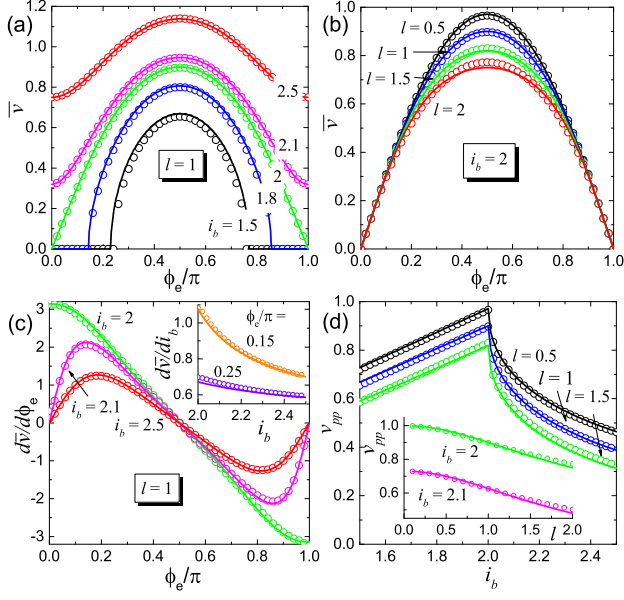


Figure 3. Comparison of results obtained using the presented analytical approach (expressions (7), (13) - solid curves) and using numerical calculations of system (1) (dots). (a) SQUID voltage response $\bar{v}(\phi_e)$ at $l = 1$ for a set of the bias currents $i_b = 1.5, 1.8, 2, 2.1, 2.5$. (b) The voltage response at $i_b = 2$ for a set of the inductance values $l = 0.5, 1, 1.5, 2$. (c) SQUID transfer function $\partial\bar{v}/\partial\phi_e$ for the bias current values $i_b = 2, 2.1, 2.5$; inset shows the dynamic resistance $\partial\bar{v}/\partial i_b$ for the external flux values $\phi_e = 0.15, 0.25$; $l = 1$. (d) The voltage response amplitude v_{pp} versus the bias current for the inductance values $l = 0.5, 1, 1.5$; inset presents the amplitude versus the inductance at the bias currents $i_b = 2, 2.1$.

voltage drop on the two shunt resistors connected in parallel.

For the bias current equal to the critical current $i_b = 2$ the voltage response amplitude decreases with the inductance as

$$v_{pp} = 1 - \frac{l^2}{2l^2 + 8}. \quad (14)$$

With inductance increase this amplitude tends to $v_{pp} \rightarrow 0.5$. At the same time, according to (10), the circulating current amplitude tends to zero for $l \rightarrow \infty$, and so $v_{pp} \rightarrow 0$. Therefore this dependence of the amplitude on the inductance $v_{pp}(l)$ (14) is relevant only in the frame of validity of the proposed approach i.e. for $l \leq 1$.

2.3. Comparison with numerical calculations

Figure 3 shows curves calculated using the presented analytical approach (expressions (7), (13) - solid lines) and obtained using numerical calculations of system (1) (dots).

Figure 3(a) presents SQUID voltage responses for the inductance value $l = 1$. It is seen that the curves calculated using both analytical and numerical approaches are well consistent in the wide bias current

range $i_b = 1.5 \dots 2.5$ around the SQUID critical current.

Equation (5) shows that amplitude of the difference phase oscillations is proportional to $\psi_{\sim}^A \sim -\sin \phi_e$, and so the inductance mainly affects middle part of the voltage response. Increase of the inductance leads to increase of $\psi_{\sim}^A \sim -li_{cir}^a/2$ and violation of assumption that $\psi_{\sim} \ll 1$. This is seen as small deviation of the analytical curves from the numerical ones in Fig. 3(b) for $l > 1$.

We should note that expression (7) for the voltage response allows one to calculate all related curves like the transfer function $\partial\bar{v}/\partial\phi_e$ or the dynamic resistance $\partial\bar{v}/\partial i_b$ presented in figure 3(c) and its inset correspondingly.

Fig. 3(d) presents the voltage response amplitude dependencies on the bias current and on the inductance. Comparing analytical and numerical data we conclude that within the area of its applicability presented approach describes SQUID voltage characteristics fairly well.

3. SQUID current

This Section is devoted to consideration of symmetrical SQUID current response. The response is first considered in superconducting state for arbitrary SQUID inductance. Consideration of the response in resistive state is conducted for $l \leq 1$ using expression (8) for the circulating current obtained in the previous Section.

3.1. Superconducting state

Time derivatives of the sum and difference phases $\dot{\theta}$, $\dot{\psi}$ as well as oscillating part of the difference phase ψ_{\sim} in superconducting state is zero. Expression for the circulating current in this case is given as

$$i_{cir} = \sin \psi \cos \theta, \quad (15)$$

which can be combined with (1b) to produce

$$i_{cir} = \sqrt{\cos^2 \psi - \frac{i_b^2}{4}} \tan \psi. \quad (16)$$

This expression can be readily used in the case of vanishing inductance $l \rightarrow 0$ with $\psi = -\phi_e$. For zero bias current it simplifies further

$$i_{cir} = -\text{sgn}(\cos \phi_e) \sin \phi_e. \quad (17)$$

For small but nonzero inductances the circulating current was derived in the frame of perturbation analysis, to first [41] and second [40] order in the inductance. However, for the inductance value $l \approx 1$ numerical calculation result becomes inconsistent compared to Ref. [40, 41].

To find the circulating current for arbitrary inductance one has to solve an equation $f(\psi) = 0$ for transcendental function

$$f(\psi) = \frac{l}{2} \sqrt{\cos^2 \psi - \frac{i_b^2}{4}} \tan \psi + \psi + \phi_e \quad (18)$$

derived from (1a), and substitute the found difference phase into expression (16). In general case the solution can be found using the following quasianalytical approach.

The method is based on integral definition of root x_0 of arbitrary continuous function $f(x)$ having just one zero in the range of interest $[a, b]$:

$$x_0 = a + \int_a^b \text{H}[-\text{sgn}(f[a])] + \text{sgn}(f[a]) \text{H}[f(x)] dx, \quad (19)$$

where $\text{H}(x)$ is the Heaviside step function. Since period of current modulation corresponds to the range $\phi_e \in [0, \pi]$, root of function $f(\psi)$ has to be sought in the range $\psi_0 \in [0, -\pi]$. However, function $f(\psi)$ is undefined inside the region $|\cos \psi| < i_b/2$, and can have up to three zeros depending on the parameters i_b , l , ϕ_e .

The first obstacle can be overcome by equalizing function $f(\psi)$ to the mean f_m of its boundary values inside the region $|\cos \psi| \leq i_b/2$, which is obviously $f_m = \text{sgn}(\psi) \text{ceil}(|\psi|/\pi)\pi/2 + \phi_e$, where $\text{ceil}(x)$ is the ceiling function. In such complementary definition function $f(\psi)$ is shown in Fig. 4. It is seen from (18) that ϕ_e just shifts function $f(\psi)$ along the ordinate axis.

If function $f(\psi)$ is not monotonic (depending on l , i_b), the dependence $\psi_0(\phi_e)$ is hysteretic. In this case the function can have more than one root for a certain ϕ_e . To find proper root, integral (19) should be taken from the starting point a up to the local extremal point closest to a (ψ^\uparrow for ϕ_e variation $\phi_e^\uparrow = 0 \dots \pi$ and ψ^\downarrow for $\phi_e^\downarrow = \pi \dots 0$, see inset in Fig. 4) if the function f at these points ($f(a)$ and $f(\psi^{\uparrow\text{or}\downarrow})$) is of the opposite sign. Otherwise the limits of integration should be leaved unchanged.

Alteration of the integral upper limit b can be formalized as follows:

$$b(\phi_e^{\uparrow\downarrow}) = b + \text{H}[-f(a)\text{f}^{\uparrow\downarrow}(\phi_e)](\psi^{\uparrow\downarrow} - b), \quad (20)$$

where

$$\text{f}^{\uparrow\downarrow}(\phi_e) = \begin{cases} f(\psi^{\uparrow\downarrow}; \phi_e) & \text{if } \psi^{\uparrow\downarrow} \neq -\pi/2, \\ \mp l/2 - \pi/2 + \phi_e & \text{otherwise.} \end{cases}$$

The reason of such definition of $\text{f}^{\uparrow\downarrow}$ is the fact that at $i_b = 0$ the function f has a form

$$f(\psi) = \frac{l}{2} \text{sgn}(\cos \psi) \sin \psi + \psi + \phi_e, \quad (21)$$

which corresponds to the leap at $\psi^\uparrow = \psi^\downarrow = -\pi/2$. Thus we put $\text{f}^{\uparrow\downarrow}$ equal to the margin values of f function in vicinity of the leap.

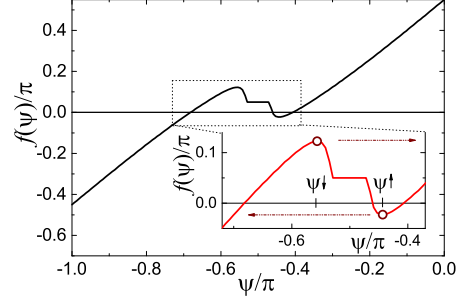


Figure 4. Transcendental function $f(\psi)$ (18) complementary defined inside the region $|\cos \psi| < i_b/2$, which implicitly defines the difference phase in superconducting state; $i_b = 0.2$, $l = 1$, $\phi_e = 0.55\pi$. Inset zooms the function nonlinear part forming hysteresis at $\psi_0(\phi_e)$ and $i_{cir}(\phi_e)$ dependencies. Dots show local extrema of $f(\psi)$ function.

For $i_b > 0$ coordinates ψ^\uparrow , ψ^\downarrow can be found using derivative of $f(\psi)$ function

$$\frac{\partial f}{\partial \psi} = -\frac{\frac{1}{2} \sin^2 \psi}{\sqrt{\cos^2 \psi - \frac{i_b^2}{4}}} + \frac{\frac{l}{2} \sqrt{\cos^2 \psi - \frac{i_b^2}{4}}}{\cos^2 \psi} + 1 \quad (22)$$

and formula (19)

$$\psi^\uparrow = \int_0^{-\arccos \frac{i_b}{2}} \text{H} \left[\frac{\partial f(\phi)}{\partial \phi} \right] d\phi, \quad (23a)$$

$$\psi^\downarrow = -\pi - \psi^\uparrow. \quad (23b)$$

Note, that $f(\psi^\uparrow) - f(\psi^\downarrow)$ defines the width of $\psi_0(\phi_e)$ and $i_{cir}(\phi_e)$ hysteresis.

$\psi_0(\phi_e)$ dependencies for both directions of ϕ_e variation can be obtained as follows:

$$\psi_0(\phi_e^\uparrow) = \int_0^{-\pi + \text{H}[-\text{f}^\uparrow(\phi_e)](\psi^\uparrow + \pi)} \text{H}[f(\phi; \phi_e^\uparrow)] d\phi, \quad (24a)$$

$$\psi_0(\phi_e^\downarrow) = -\pi + \int_{-\pi}^{\text{H}[\text{f}^\downarrow(\phi_e)]\psi^\downarrow} 1 - \text{H}[f(\phi; \phi_e^\downarrow)] d\phi. \quad (24b)$$

These dependencies (24) and corresponding circulating currents obtained by expression (16), as well as corresponding data obtained by numerical calculations of system (1) are presented in Fig. 5. Because of quasi-analytical nature of the presented approach the data obtained using expressions (24), (16) are perfectly consistent with the ones calculated numerically.

Increase of the inductance value clearly leads to enlargement of the hysteresis (see Fig. 5(a),(c)) since inductance is the amplitude of non-monotonic term of f function. Physical meaning of this fact is as follows. For zero bias current and vanishing inductance $l \rightarrow 0$ a fluxon penetrates into the SQUID at $\Phi_e = \Phi_0/2$ that is accompanied by changing of the circulating current flow direction (17). The current flow through a finite inductance produces additional magnetic flux, and so

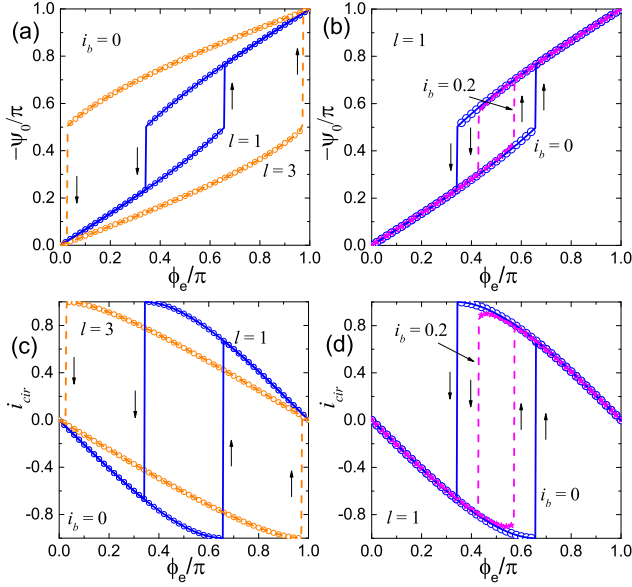


Figure 5. The difference phase ψ_0 versus the external flux ϕ_e calculated using expressions (24) (solid lines) for (a) the bias current value $i_b = 0$ and the inductance values $l = 1, 3$, and for (b) $i_b = 0, 0.2, l = 1$. (c), (d) The circulating current corresponding to the curves shown in (a), (b) panels calculated using expression (16) (solid lines). The same dependencies obtained using numerical calculations of system (1) in all panels are presented by dots. Vertical arrows show direction of variation of the functions.

the external flux can be screened without penetration of a fluxon into the SQUID loop up to higher values (Fig. 5(c)). The inductance value $l = \pi$ corresponds to the case where a fluxon penetrates into the SQUID at $\Phi_e = \Phi_0$. Starting from this inductance value the circuit has two stable states at zero applied flux (with and without a fluxon inside it), and thus the loop is called “quantizing” one.

At the same time, increase of the bias current leads to widening of the range where the f function is initially undefined and decrease of the range where it is non-monotonic. Physically, this means that the bias current flowing through the junctions allows smaller circulating current in the superconducting state. This shrinks the hysteresis (see Fig. 5(b),(d)) and finally results in formation of the region of resistive state.

3.2. Resistive state

Time averaging of (8) leads to the following expression for the averaged circulating current in resistive state:

$$\bar{i}_{cir} = -\frac{2lw_{J-}}{l^2w_{J-}^2 + 4} \left(\frac{i_b}{2} - w_{J-} \right) \tan \psi_-. \quad (25)$$

Taking $\psi_- = -\phi_e$ we calculated current curves presented in Fig. 6 by solid lines. Corresponding curves calculated numerically using system (1) are shown by dots.

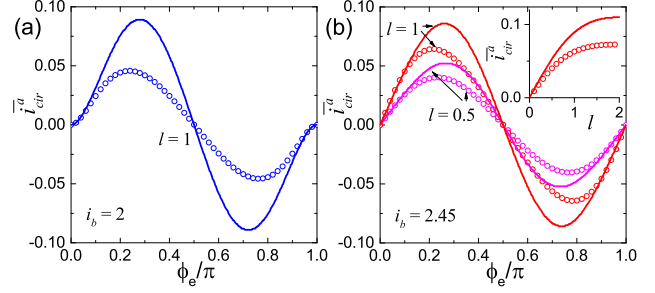


Figure 6. The averaged circulating current \bar{i}_{cir} versus the external flux ϕ_e calculated using expression (25) with $\psi_- = -\phi_e$ (solid lines) and obtained by numerical calculations of system (1) (dots). (a) $i_b = 2, l = 1$. (b) $i_b = 2.45, l = 0.5, 1$; inset shows the averaged current at $\phi_e = \pi/4$ versus the inductance calculated using (27) (solid line) and numerically (dots).

Zero value of the averaged current at $\phi_e = 0, \pi$ corresponds to an absent or purely harmonic circulating current, according to (8). Nonzero averaged current at $\phi_e \approx \pi/4$ appears due to unharmonic shape of the circulating current which is not accurately described with proposed linearization of the equations (1). While consistency for the bias current $i_b = 2$ is only qualitative (Fig. 6(a)), for higher bias current value it is improved (Fig. 6(b)). The reason is decrease of oscillating part of the difference phase ψ_- (5).

Simplifying expression (25) at the point $\phi_e = \pi/4$, one can estimate the averaged circulating current amplitude \bar{i}_{cir}^a ,

$$\bar{i}_{cir}^a = \frac{2l\sqrt{i_b^2 - 2} \left(i_b - \sqrt{i_b^2 - 2} \right)}{l^2(i_b^2 - 2) + 16}. \quad (26)$$

For the bias current value $i_b = \sqrt{6} \approx 2.45$ the amplitude is approximately

$$\bar{i}_{cir}^a \approx \frac{0.45l}{l^2 + 4}. \quad (27)$$

Corresponding curve $\bar{i}_{cir}^a(l)$ is shown in inset of Fig. 6(b) with numerical data for comparison.

4. SQUID with small spread of parameters

In this Section we study effect of reasonable technological spread of parameters ($\Delta I_c, \Delta R_n$ up to $\pm 20\%$, and arbitrary inequality of SQUID inductive shoulders) on the SQUID responses. Such spread may result in a small asymmetry of the SQUID.

The considered DC SQUID is shown in Fig. 7. The asymmetry is presented by inequality of the inductive shoulders $l_1 \neq l_2, l_1 + l_2 = l$, and differences of the critical currents and shunt resistances $i_{c1} \neq i_{c2}, r_{n1} \neq r_{n2}$ of the junctions. We assume below that $|i_{c1} - i_{c2}| \ll 1, |r_{n1} - r_{n2}| \ll 1$, and that the bias current is of the order of the SQUID critical current $i_b \approx i_{c1} + i_{c2}$.

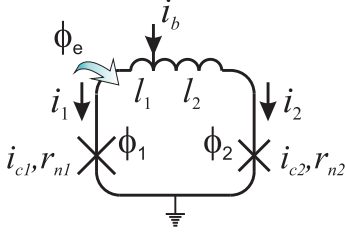


Figure 7. DC SQUID with asymmetry presented by inequality of the inductances $l_1 \neq l_2$, critical currents $i_{c1} \neq i_{c2}$, and shunt resistances $r_{n1} \neq r_{n2}$.

4.0.1. Asymmetry of the inductive shoulders. Simplest case of SQUID asymmetry is inequality of the inductances $l_1 \neq l_2$. If $i_{c1} = i_{c2}$, $r_{n1} = r_{n2}$ then modification appears only in equation (1a). Phase drop on the inductances $l_1 i_1 - l_2 i_2$ rewritten as $(i_b/2)[l_1 - l_2] + (l/2)[i_1 - i_2]$ converts this equation into the following one:

$$\frac{\Sigma l}{2} \dot{\psi} = - \left(\psi + \phi_e + \frac{i_b \Delta l}{2} \right) - \frac{\Sigma l}{2} \sin \psi \cos \theta, \quad (28)$$

where $\Sigma l = l_1 + l_2$, $\Delta l = l_1 - l_2$.

It is seen that this asymmetry can be accounted just by the constant offset $i_b \Delta l / 4$ to the external flux ϕ_e , which appears due to the bias current flow through the part of inductance Δl . In consideration of asymmetries of the critical currents and shunt resistances we first put $\Delta l = 0$ for simplicity, and then generalize obtained results for arbitrary Δl .

4.0.2. Asymmetry of the critical currents and shunt resistances. The spread in critical currents of Josephson junctions and shunt resistances affects system (1) noticeably, and these equations can be rewritten as

$$\frac{l}{\Sigma r_n} \dot{\psi} = -(\psi + \phi_e) + \frac{l}{2} \frac{i_b \Delta r_n}{\Sigma r_n} - \frac{l}{\Sigma r_n} \left(\frac{\Sigma v_c}{2} \sin \psi \cos \theta + \frac{\Delta v_c}{2} \cos \psi \sin \theta \right), \quad (29a)$$

$$\dot{\theta} = \frac{i_b \Sigma r_n}{2} \frac{\Sigma r_n}{2} - \frac{\psi + \phi_e}{l} \Delta r_n - \frac{\Sigma v_c}{2} \cos \psi \sin \theta - \frac{\Delta v_c}{2} \sin \psi \cos \theta. \quad (29b)$$

Here $v_c = i_c r_n$ is the characteristic voltage, $\Sigma v_c = v_{c1} + v_{c2}$, $\Delta v_c = v_{c1} - v_{c2}$, $\Sigma r_n = r_{n1} + r_{n2}$, $\Delta r_n = r_{n1} - r_{n2}$.

Below we first consider influence of this asymmetry on the voltage response and then describe its effect on the circulating current. The difference phase is again presented as a sum of constant ψ_-^* and oscillating ψ_{\sim}^* parts, where the last one is assumed to be small $\psi_{\sim}^* \ll 1$.

4.1. Voltage on SQUID with small asymmetry

4.1.1. Solution for $\psi = \psi_-^$.* Even in the absence of the asymmetry of the inductive shoulders asymmetry of the critical currents and shunt resistances still leads to a constant offset of the external flux. This offset can be found by time averaging of equation (29a) at $\dot{\phi}_e = 0$ and $i_b \approx 2$, assuming that $i_{c1,2}, r_{n1,2} \approx 1$. Since $\dot{\psi}_- = 0$, $\cos \theta = 0$, and $\sin \theta = [(i_b/2) - w_{J-}] / \cos \psi_- \approx 1$, under the made assumptions the difference phase is

$$\psi_-^* = -\phi_e - \frac{l}{2} \left[\frac{\Delta i_c}{2} - \frac{i_b - \Sigma i_c}{2} \frac{\Delta r_n}{\Sigma r_n} \right], \quad (30)$$

where $\Sigma i_c = i_{c1} + i_{c2}$, $\Delta i_c = i_{c1} - i_{c2}$.

The asymmetries Δi_c and Δr_n provide redistribution of the bias current toward the junction with larger i_c but smaller r_n . Corresponding terms enter in (30) with opposite signs accordingly. Effect due to asymmetry of the shunt resistances refers to resistive state that is manifested by prefactor proportional to the bias current deviation from the SQUID critical current $i_b - \Sigma i_c$.

To find the sum phase it is convenient to present equation (29b) in the following form:

$$\dot{\theta} = \frac{i_b \Sigma r_n}{2} \frac{\Sigma r_n}{2} - \frac{\psi + \phi_e}{l} \Delta r_n - \sqrt{\frac{\Delta v_c^2}{4} + v_{c1} v_{c2} \cos^2 \psi} \times \sin \left(\theta + \arctan \left[\frac{\Delta v_c}{\Sigma v_c} \tan \psi \right] \right). \quad (31)$$

Structure of this equation is quite analogous to the one of equation (1b), and so its solution replicates equation (2). The only difference here is the shift of the sum phase:

$$\tan \frac{\theta + c}{2} = z^* + \sqrt{1 - z^{*2}} \tan \frac{i_b^* \sqrt{1 - z^{*2}} \tau}{2}, \quad (32)$$

where

$$\frac{i_b^*}{2} = \frac{i_b \Sigma r_n}{2} + \left[\frac{\Delta i_c}{2} - \frac{i_b - \Sigma i_c}{2} \frac{\Delta r_n}{\Sigma r_n} \right] \frac{\Delta r_n}{2},$$

$$z^* = \frac{2}{i_b^*} \sqrt{\frac{\Delta v_c^2}{4} + v_{c1} v_{c2} \cos^2 \psi_-^*},$$

$$c = \arctan \left[\frac{\Delta v_c}{\Sigma v_c} \tan \psi_-^* \right].$$

The Josephson frequency similarly follows from equation (32):

$$w_{J-}^* = \sqrt{v_{c1} v_{c2}} \times \sqrt{\frac{[(i_b - i_{c1})r_{n1} + v_{c2}][(i_b - i_{c2})r_{n2} + v_{c1}]}{i_{c1} i_{c2} \Sigma r_n^2} - \cos^2 \psi_-^*}, \quad (33)$$

where w_{J-}^* should be put zero if the expression under the second square root is negative.

Here the square root of the characteristic voltage product $v_{c1}v_{c2}$ is a natural scaling factor for the voltage. Presenting this factor as

$$\sqrt{v_{c1}v_{c2}} = \frac{\sqrt{(\Sigma i_c^2 - \Delta i_c^2)(\Sigma r_n^2 - \Delta r_n^2)}}{4}, \quad (34)$$

we note that the differences of the critical currents and shunt resistances provide similar contributions.

Considering the first term under the second square root of expression (33) as squared effective bias current divided by the squared SQUID critical current

$$\frac{i_{b_{eff}}^2}{\Sigma i_c^2} = \frac{[(i_b - i_{c1})r_{n1} + v_{c2}][(i_b - i_{c2})r_{n2} + v_{c1}]}{i_{c1}i_{c2}\Sigma r_n^2}, \quad (35)$$

by analogy with expression (3), one can study how this ratio differs from the one for symmetrical case.

For identification of effect of the critical current difference on this ratio it is convenient to put difference of the shunt resistances equal to zero $\Delta r_n = 0$ and $\Sigma r_n = 2$. In this case the considered ratio is

$$\frac{i_{b_{eff}}^2}{\Sigma i_c^2} = \frac{i_b^2 - \Delta i_c^2}{\Sigma i_c^2 - \Delta i_c^2}, \quad (36)$$

and the squared effective bias current is

$$i_{b_{eff}}^2 = i_b^2 + \frac{\Delta i_c^2}{\Sigma i_c^2 - \Delta i_c^2} (i_b^2 - \Sigma i_c^2). \quad (37)$$

It is seen that asymmetry of the critical currents Δi_c affects both i_b and Σi_c (36). This results in tiny deviation of $i_{b_{eff}}^2$ from i_b^2 proportional to the asymmetry in square, and multiplied by deviation of the squares of the bias current from the SQUID critical current (37).

Consideration of shunt resistance difference at $\Delta i_c = 0$, $\Sigma i_c = 2$ leads to the following expression

$$\frac{i_{b_{eff}}^2}{4} = \frac{i_b^2}{4} - \left(\frac{i_b - 2}{2}\right)^2 \frac{\Delta r_n^2}{\Sigma r_n^2}. \quad (38)$$

Difference of the shunt resistances affects the effective bias current in accordance with the bias current redistribution (see also (30)). In comparison with the effect provided by difference of the critical currents, here the deviation of $i_{b_{eff}}^2$ from i_b^2 is even smaller (since $i_b^2 - \Sigma i_c^2 > (i_b - \Sigma i_c)^2$ for $i_b > i_c$, see (37), (38)).

Obtained results (30), (37), (38) allow us to conclude that at $i_b \approx \Sigma i_c$ the Josephson oscillation frequency is approximately equal to

$$w_{J0}^* \approx \sqrt{v_{c1}v_{c2}} \sqrt{1 - \cos^2 \left(\phi_e + \frac{l \Delta i_c}{2} \right)}, \quad (39)$$

and the asymmetries Δi_c , Δr_n mainly scale the averaged voltage and provide offset to the external flux corresponding to Δi_c .

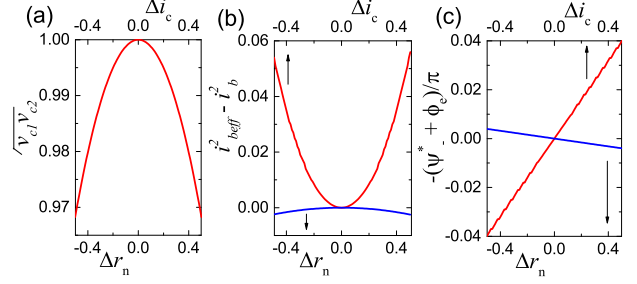


Figure 8. (a) Scaling factor $\sqrt{v_{c1}v_{c2}}$ for the averaged voltage (33), (b) deviation of the squared effective bias current from the squared bias current $i_{b_{eff}}^2 - i_b^2$, and (c) offset to the bias flux $-(\psi_-^* + \phi_e)/\pi$ versus Δr_n at $\Delta i_c = 0$, and versus Δi_c at $\Delta r_n = 0$; $\Sigma i_c, \Sigma r_n = 2, i_b = 2.2$.

Considered effects of asymmetries of the critical currents and shunt resistances on the scaling factor $\sqrt{v_{c1}v_{c2}}$, the deviation of $i_{b_{eff}}^2$ from i_b^2 , and the bias flux offset are illustrated in Fig. 8.

4.1.2. Solution for $\psi = \psi_-^ + \psi_+^*$.* Impact of oscillating current circulating in the SQUID can be introduced by oscillating part of the difference phase. Substitution of $\psi = \psi_-^* + \psi_+^*$ into equation (29a) leads to

$$\begin{aligned} \frac{l}{\Sigma r_n} \psi_+^* &= -\psi_+^* + \frac{l}{2} \left[\frac{\Delta i_c}{2} + \frac{\Sigma i_c \Delta r_n}{2 \Sigma r_n} \right] \\ &- \frac{l}{\Sigma r_n} \left(\frac{\Sigma v_c}{2} \sin \psi_-^* \cos \theta + \frac{\Delta v_c}{2} \cos \psi_-^* \sin \theta \right). \quad (40) \end{aligned}$$

It is hard to derive exact analytical solution of this equation, while approximate solution can be drawn rather easy assuming $l \ll 1$ and putting $\dot{\theta} \approx \bar{\theta} = w_{J-}^*$:

$$\begin{aligned} \psi_+^* &= \frac{l}{2} \left[\frac{\Delta i_c}{2} + \frac{\Sigma i_c \Delta r_n}{2 \Sigma r_n} \right] - \frac{l}{\Sigma r_n \sqrt{1 + \left[\frac{l w_{J-}^*}{\Sigma r_n} \right]^2}} \\ &\times \left[\frac{\Sigma v_c}{2} \sin \psi_-^* \cos \left(\theta - \arctan \left[\frac{l w_{J-}^*}{\Sigma r_n} \right] \right) \right] \\ &+ \frac{\Delta v_c}{2} \cos \psi_-^* \sin \left(\theta - \arctan \left[\frac{l w_{J-}^*}{\Sigma r_n} \right] \right). \quad (41) \end{aligned}$$

To find the correction w_{J-}^* of the Josephson frequency we substitute the found difference phase $\psi = \psi_-^* + \psi_+^*$ (30), (41) into equation (29b):

$$\begin{aligned} w_{J-}^* &= -\frac{\overline{\psi_+^*}}{l} \Delta r_n \\ &+ \frac{\Sigma v_c}{2} \sin \psi_-^* (\overline{\psi_+^*} \sin \theta) - \frac{\Delta v_c}{2} \cos \psi_-^* (\overline{\psi_+^*} \cos \theta). \quad (42) \end{aligned}$$

Since ψ_+^* is proportional to the inductance (41), the last two terms in (42) represent SQUID LR -filtering of

the circulating current. They vanish in the limit $l \rightarrow 0$. At the same time, for $l = 0$ the first term is non zero representing difference of voltage drops of the time-averaged circulating current on the shunt resistors.

Unfortunately, full expression for $w_{J\sim}^*$ is rather complicated

$$w_{J\sim}^* = -\frac{\frac{l}{\Sigma r_n} \frac{i_b^*}{2} \left(\frac{lw_{J-}^*}{\Sigma r_n} v_{c1}^2 v_{c2}^2 \sin^2 2\psi_-^* + K_1 + K_2 \right)}{4 \left(\left[\frac{lw_{J-}^*}{\Sigma r_n} \right]^2 + 1 \right) \left[\frac{i_b^{*2}}{4} - w_{J-}^{*2} \right] \left(\frac{i_b^*}{2} + w_{J-}^* \right)} + K_3. \quad (43)$$

Here the coefficients $K_{1,2,3}$ have following forms

$$K_1 = \frac{v_{c1} v_{c2}}{i_b^*} \left[\Sigma v_c \Delta v_c - 4w_{J-}^* \frac{\Delta r_n}{\Sigma r_n} \left(\frac{i_b^*}{2} + w_{J-}^* \right) \right] \times \left(\frac{i_b^*}{2} - w_{J-}^* \right) \sin 2\psi_-^*,$$

$$K_2 = \frac{\Sigma v_c \Delta v_c}{i_b^*} \left[\frac{w_{J-}^{*2}}{2} \frac{l}{\Sigma r_n} \Sigma v_c \Delta v_c - 2 \frac{\Delta r_n}{l} \left(\frac{i_b^{*2}}{4} - w_{J-}^{*2} \right) \right],$$

$$K_3 = \frac{l}{2} \left(\frac{\Delta i_c}{2} + \frac{\Sigma i_c \Delta r_n}{2 \Sigma r_n} \right) \left[\frac{v_{c1} v_{c2}}{2} \frac{\sin 2\psi_-^*}{\left(\frac{i_b^*}{2} + w_{J-}^* \right)} - \frac{\Delta r_n}{l} \right].$$

They arise due to asymmetry of the SQUID parameters.

Amplitude of the voltage response can be found through the total Josephson frequency $w_J^* = w_{J-}^* + w_{J\sim}^*$ taken at $\psi_-^* = -\pi/2$ and $\psi_-^* = 0$. For the bias current equal to the SQUID critical current $i_b = \Sigma i_c$ this amplitude is

$$v_{pp}^* = \sqrt{v_{c1} v_{c2}} - \frac{\Sigma v_c}{4} \times \left[\frac{v_{c1} v_{c2} \frac{l^2}{\Sigma r_n^2} \Sigma v_c - \frac{\Delta r_n}{\Sigma r_n} \Delta v_c}{\left(\sqrt{v_{c1} v_{c2}} + \frac{\Sigma v_c}{2} \right) \left[v_{c1} v_{c2} \frac{l^2}{\Sigma r_n^2} + 1 \right]} + \frac{2 \Delta r_n \Delta v_c}{\Sigma r_n \Sigma v_c} \right]. \quad (44)$$

For symmetrical case this expression takes the form of (14) with according scaling coefficients.

Note, that for $l = 0$ this amplitude (44) is

$$v_{pp}^* = \sqrt{v_{c1} v_{c2}} - \frac{\Delta v_c \Delta r_n}{2 \Sigma r_n} \left(1 - \frac{\Sigma v_c}{\Sigma v_c + 2 \sqrt{v_{c1} v_{c2}}} \right). \quad (45)$$

The last term in (45) represents deviation of the voltage response amplitude corresponding to the first term of (42). For zero difference of the shunt resistances $\Delta r_n = 0$ this term is zero. At the same time, for zero difference of the critical currents $\Delta i_c = 0$ ($\Delta v_c = \Sigma i_c \Delta r_n / 2$) this deviation is proportional to Δr_n^2 . In this case the difference of shunt resistances always leads to additional decrease of the voltage response. We will return to consideration of this fact below in Section devoted to time-averaged circulating current.

4.1.3. Generalization to the case of unequal inductive shoulders. Since asymmetry of the inductances $l_1 \neq l_2$ just shifts the bias flux, it can be accounted by according addition $i_b \Delta l / 4$ to the expression for the constant difference phase (30)

$$\psi_-^* = -\phi_e - \frac{i_b \Delta l}{2} \frac{\Delta l}{2} - \frac{\Sigma l}{2} \left[\frac{\Delta i_c}{2} - \frac{i_b - \Sigma i_c \Delta r_n}{2 \Sigma r_n} \right], \quad (46)$$

and substitution of the total inductance Σl instead of l in equation (40) and subsequent expressions (41)-(44).

Voltage response

$$\bar{v}^* = w_J^* = w_{J-}^* + w_{J\sim}^* \quad (47)$$

(where w_J^* should be put zero if $w_{J-}^* = 0$) can be found by combining expressions (33), (43), and (46). The responses calculated from these expressions for a chosen set of parameters $i_b = 2$, $\Sigma i_c = 1.9$, $\Delta i_c = -0.3$, $\Sigma r_n = 2.05$, $\Delta r_n = 0.35$, $\Sigma l = 1$, and $\Delta l = 0, -0.8$ are shown in Fig. 9(a) by solid lines, while the data obtained by numerical calculations of system (29) are presented by dots. It is seen that the data are well consistent despite the fact that oscillating part of the difference phase (41) is found approximately. Even for $\Delta l = 0$ the voltage response has small constant shift along ϕ_e axis due to Δi_c , Δr_n asymmetries, in accordance with (46). Corresponding terms arising in (42) provide some asymmetry of the voltage response shape which is though quite small for considered case $|\Delta i_c|, |\Delta r_n| \ll 1$.

Figure 9(b) illustrates effects of the critical current difference Δi_c at $\Delta r_n = 0$ and difference of the shunt resistances Δr_n at $\Delta i_c = 0$ on the amplitude of the voltage response v_{pp}^* for $i_b, \Sigma i_c, \Sigma r_n = 2$ and $l = 1$. Corresponding curves are calculated using (44) and shown by lines. The dependence $v_{pp}^* = v_{pp} \sqrt{v_{c1} v_{c2}}$, which can be derived from the amplitude v_{pp} in symmetrical case (14) and the voltage scaling factor (34) is presented by dots.

Consistency of the curves indicates that individual effect of the critical current difference reduces to the voltage scaling. For small inductance values ($l \ll 1$) expression (44) can be approximated by

$$v_{pp}^* \approx \sqrt{1 - \frac{\Delta i_c^2}{4}} v_{pp}. \quad (48)$$

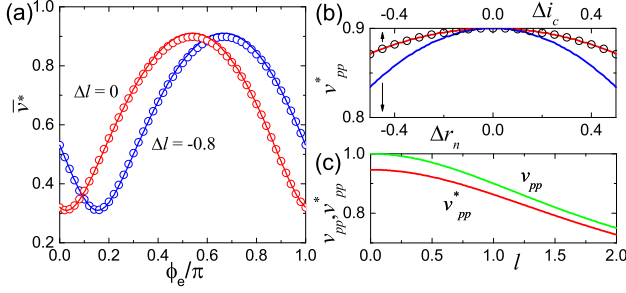


Figure 9. (a) Voltage response calculated using expression (47) (solid lines) and calculated numerically using system (29) (dots) for a set of parameters: $i_b = 2$, $\Sigma i_c = 1.9$, $\Delta i_c = -0.3$, $\Sigma r_n = 2.05$, $\Delta r_n = 0.35$, $\Sigma l = 1$, and $\Delta l = 0$, -0.8 . (b) Voltage response amplitude v_{pp}^* versus Δi_c at $\Delta r_n = 0$, and versus Δr_n at $\Delta i_c = 0$ (solid lines) for $i_b, \Sigma i_c, \Sigma r_n = 2$ and $l = 1$. Approximate dependence $v_{pp}^* = v_{pp} \sqrt{v_{c1} v_{c2}}$ derived from (14), (34) is shown by dots. (c) Voltage response amplitude v_{pp}^* for the same set of parameters as the ones taken for panel (a) but $i_b = \Sigma i_c$ calculated using expression (44), and the amplitude v_{pp} for symmetrical case at $i_b = 2$ calculated using expression (14) versus the inductance.

At the same time, individual effect of difference of the shunt resistances includes additional decrease of v_{pp}^* due to time-averaged voltage drop of the circulating current on Δr_n that leads to

$$v_{pp}^* \approx \sqrt{1 - \frac{\Delta r_n^2}{4} v_{pp} - \frac{\Delta r_n^2 l^2 + 2}{4 l^2 + 4}}. \quad (49)$$

Note, that decrease of the amplitude v_{pp}^* resulting from LR -filtering not precisely follows v_{pp} (14). Therefore obtained expressions (48), (49) are relevant only for $l \ll 1$. In general, the circulating current-time dependence, which is purely harmonic in symmetrical case at $\psi_- = -\pi/2$ is unharmonic at $\psi_-^* = -\pi/2$ for $\Delta v_c \neq 0$. This can be seen from expressions (32), (41). The current-time dependence becomes inclined (at $\psi_-^* = -\pi/2$) due to different rates of switching of the junctions $v_{c1} \neq v_{c2}$. Figure 9(c) presents the voltage response amplitude $v_{pp}^*(l)$ calculated using expression (44) for the same parameters as the ones taken for Fig. 9(a) but $i_b = \Sigma i_c$. It is compared with the amplitude v_{pp} of symmetrical SQUID (14) versus the total inductance. Inconstancy of the difference $v_{pp}^* - v_{pp}$ illustrates slight changes in the circulating current and conditions of its filtering provided by asymmetry.

4.2. Circulating current in SQUID with small asymmetry

4.2.1. Superconducting state. Effect of the asymmetries on the circulating current in superconducting state $\dot{\theta}, \dot{\psi} = 0$ can be easily found for $i_b = 0$ by combining equations (29). Since for zero bias current inequality of the inductive shoulders plays no role, we consider here only effects of differences of the critical currents and shunt resistances. The $f(\psi)$ function (21)

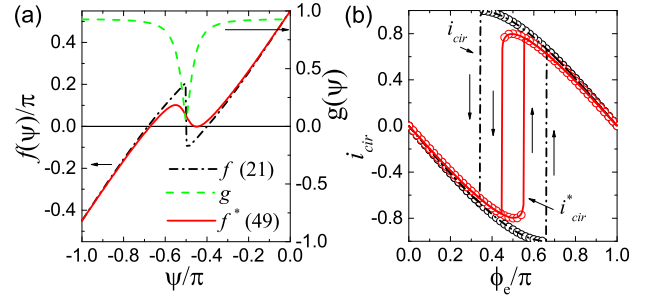


Figure 10. (a) Transcendental function f for symmetrical SQUID (21), $g(\psi)$ factor affecting its nonlinear term in asymmetrical case, and $f^*(\psi)$ function (50) for asymmetrical SQUID with parameters $\Sigma i_c = 1.9$, $\Delta i_c = -0.3$, $\Sigma r_n = 2.05$, $\Delta r_n = 0.35$, $l = 1$. (b) The circulating currents i_{cir} , i_{cir}^* corresponding to the functions f , f^* presented in panel (a), calculated using expressions (16), (24), (53) (lines). Numerical data obtained using system (29) are shown by dots for comparison. Vertical arrows show direction of variation of functions.

obtained from the system (29) has the following form:

$$f^*(\psi) = g(\psi) \frac{l}{2} \text{sgn}(\cos \psi) \sin \psi + \psi + \phi_e, \quad (50)$$

where

$$g(\psi) = \frac{\Sigma v_c + \Delta v_c A_I}{\Sigma r_n \sqrt{1 + A_I^2 \tan^2 \psi}} \quad (51)$$

is factor arising from asymmetry, and

$$A_I = \frac{\Sigma v_c \Delta r_n - \Delta v_c \Sigma r_n}{\Sigma v_c \Sigma r_n - \Delta r_n^2}. \quad (52)$$

Constant A_I is always equal to zero if $\Delta i_c = 0$. This means that asymmetry of the shunt resistances itself does not affect the circulating current, as it is expected for superconducting state. In this case the nonlinear term of $f(\psi)$ (21) is multiplied just by $g = \Sigma i_c / 2$. Generally, the effect of difference of the shunt resistances on $g(\psi)$ remains negligible for arbitrary Δi_c .

For equal shunt resistances $\Delta r_n = 0$ the A_I constant is $A_I = -\Delta i_c / \Sigma i_c$ and so the $g(\psi)$ function is the product of $2i_{c1}i_{c2} / \Sigma i_c$ and $1 / \sqrt{1 + (\Delta i_c / \Sigma i_c)^2 \tan^2 \psi}$. The first factor is of the order of unity for $i_{c1}, i_{c2} \approx 1$. The second factor is positive and less than unity. It has a deep at $\psi = \pi/2 + \pi n$ (where n is integer). These properties of $g(\psi)$ factors lead to effective smoothing of nonlinear bend of the $f(\psi)$ function in the vicinity of $\psi = \pi/2 + \pi n$ (see Fig. 10(a)). The bend smoothing, in turn, leads to shrinking of hysteresis of the circulating current curve illustrated in Fig. 10(b). This effect increases with increase of Δi_c . It is manifested in the manner somewhat analogous to nonzero bias current effect considered in Section 3. However, here it results from

limitation of the circulating current by smaller critical current of unequal junctions.

The $f(\psi)$, $f^*(\psi)$ functions shown in Fig. 10(a) are calculated using expressions (21), (50) for symmetrical case, and for the same parameters of SQUID asymmetry as the ones taken for calculations of the data presented in Fig. 9(a) correspondingly. The circulating currents i_{cir} , i_{cir}^* in Fig. 10(b) are found using f , f^* functions, expressions (16), (24), and derivative of $f^*(\psi)$ function

$$\frac{\partial f^*}{\partial \psi} = g(\psi) \frac{l}{2} \operatorname{sgn}(\cos \psi) \left[\cos \psi - \frac{\sin \psi \tan \psi A_J^2 (1 + \tan^2 \psi)}{1 + A_J^2 \tan^2 \psi} \right] + 1. \quad (53)$$

Numerical data shown in Fig. 10(b) are obtained using system (29).

4.2.2. *Resistive state.* Time-averaged circulating current in resistive state can be found using expressions (32), (33), (41) and (46):

$$\bar{i}_{cir}^* = \frac{\left[\Sigma v_c \Delta v_c - 2 \frac{\Sigma l w_{j-}^*}{\Sigma r_n} v_{c1} v_{c2} \sin 2\psi_-^* \right] \left(\frac{i_b^*}{2} - w_{j-}^* \right)}{2 \Sigma r_n \left(\left[\frac{\Sigma l w_{j-}^*}{\Sigma r_n} \right]^2 + 1 \right) \left[\frac{\Delta v_c^2}{4} + v_{c1} v_{c2} \cos^2 \psi_-^* \right]} - \frac{i_b \Delta r_n}{2 \Sigma r_n}. \quad (54)$$

For symmetrical case this expression converts into (25) with corresponding scaling coefficients. However, contrary to (25) here the time-averaged circulating current, in general, has some offset due to redistribution of the bias current. For the bias current equal to the SQUID critical current $i_b = \Sigma i_c$ the averaged circulating current at $\psi_-^* = 0$ is

$$\bar{i}_{cir}^* = \frac{1}{\Sigma r_n} \left(\Delta v_c - \frac{\Sigma i_c}{2} \Delta r_n \right). \quad (55)$$

For $\Delta i_c = 0$ the current is $\bar{i}_{cir}^* = 0$ as it is expected, but for $\Delta r_n = 0$ the current is $\bar{i}_{cir}^* = \Delta i_c / 2$.

Note, that in contrast with (25) the current (54) for $l = 0$ is not zero. At the peak of the voltage response $\psi_-^* = -\pi/2$ and for $i_b = \Sigma i_c$ expression (54) can be simplified if Δi_c or Δr_n is zero.

For $\Delta i_c = 0$ it is

$$\bar{i}_{cir}^* = -\frac{\Delta r_n \Sigma i_c}{2 \Sigma r_n} \left(1 - \frac{\Sigma r_n}{\Sigma r_n + 2\sqrt{r_{n1} r_{n2}}} \right). \quad (56)$$

Remembering that $\Delta v_c = \Sigma i_c \Delta r_n / 2$ and $\Sigma v_c = \Sigma i_c \Sigma r_n / 2$, one can see that (56) is just the second term of the expression (45) for the voltage response amplitude without the factor $\Delta r_n / 2$ arising from the first term of (42). Since the expression in the brackets (56) is always positive, the averaged circulating current

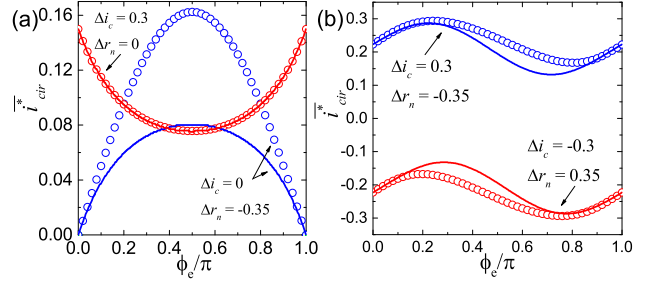


Figure 11. The averaged circulating current \bar{i}_{cir}^* versus the external flux ϕ_e calculated using expression (54) (solid lines) and obtained using numerical calculations of system (29) (dots). (a) $\Delta i_c = 0$, $\Delta r_n = -0.35$ and $\Delta i_c = 0.3$, $\Delta r_n = 0$ at $i_b = \Sigma i_c = 1.9$, $\Sigma r_n = 2.05$, $l = 0$. (b) $\Delta i_c = -0.3$, $\Delta r_n = 0.35$ and $\Delta i_c = 0.3$, $\Delta r_n = -0.35$ at $i_b = 2.45$, $\Sigma i_c = 1.9$, $\Sigma r_n = 2.05$, $\Sigma l = 1$ and $\Delta l = 0$.

in this case decreases the voltage response because it always flows toward the junction with smaller shunt resistor. Comparing (55) and (56) we conclude that the applied flux increases the averaged circulating current induced due to inequality of the shunt resistances.

For $\Delta r_n = 0$ the averaged circulating current is

$$\bar{i}_{cir}^* = \frac{\Delta i_c}{2} \frac{\Sigma i_c}{\Sigma i_c + 2\sqrt{i_{c1} i_{c2}}}. \quad (57)$$

Since the second factor in (57) is less than unity, it is seen that the applied flux decreases the averaged circulating current induced due to inequality of the critical currents (compare (55) and (57)).

Figure 11(a) presents the averaged circulating current (54) calculated for $\Delta i_c = 0$, $\Delta r_n = -0.35$ and $\Delta i_c = 0.3$, $\Delta r_n = 0$ at $i_b = \Sigma i_c = 1.9$, $\Sigma r_n = 2.05$, $l = 0$ (solid lines). Corresponding data calculated numerically using system (29) are shown by dots. It is seen that even for small absolute current values \bar{i}_{cir}^* the data corresponding to the averaged circulating current in SQUID with asymmetry of the critical currents are perfectly consistent. Although the data for SQUID with asymmetry of the shunt resistances differ noticeably at $\phi_e \approx \pi/2$ resulting from approximate solution for ψ_-^* (41), qualitative behavior is still found correctly for both asymmetries.

Figure 11(b) shows the circulating current calculated for the same set of parameters as the ones taken for Fig. 9(a) but $i_b = 2.45$ ($\Delta l = 0$), and for SQUID with inverted asymmetry of the critical currents and shunt resistances ($\Delta i_c \rightarrow -\Delta i_c$, $\Delta r_n \rightarrow -\Delta r_n$, while Σi_c , Σr_n are held the same). The data obtained by expression (54) are shown by lines, and the ones calculated numerically using (29) are presented by dots. While consistency of the curves remains to be just qualitative, the offset to the averaged circulating current is found precisely.

5. SQUID with inductance of practical device

The voltage-flux and current-flux functions obtained in Sections 2, 3 for resistive state are valid only for SQUID with small inductance $l \leq 1$. In this Section we fit numerical data for the SQUID responses by our analytical expressions introducing fitting parameters to expand the frame of validity of our approach to higher values of the inductance. This makes our expressions suitable for design process of practical SQUIDs and SQUID-based circuits.

5.1. SQUID voltage response

In Section 2 it was considered that expression (14) obtained for the voltage response amplitude is relevant only for small values of the inductance $l \leq 1$. Since the voltage \bar{v} across symmetrical SQUID at $i_b = 2$ and $\phi_e = 0$ is zero, the response amplitude is just \bar{v} at $\phi_e = \pi/2$. Comparison of dependencies $\bar{v}(l)$ calculated using (14) and obtained by numerical calculations of system (1) is shown in Fig. 12. It is seen that proposed linearization of (1) leads to inaccurate determination of the voltage response amplitude for $l > 1$ that limits application of the derived expressions. To make our approach useful in practical circuits design we propose usage of expression (7) for SQUID voltage response with fitting parameters which can be found from numerical calculations of (1) as follows.

Dependence of the voltage on the inductance $\bar{v}(l)$ at $i_b = 2$, $\phi_e = \pi/2$ obtained by numerical calculations of (1) and presented in Fig. 12 can be well approximated by function

$$\bar{v}_{\pi/2}^{num} = 1 - p, \quad (58)$$

where

$$p = \frac{l^{1.66}}{2.44l^{1.48} + 7.22}. \quad (59)$$

The voltages (14) and (58) can be equalized with introduction of effective inductance l_a :

$$1 - \frac{l_a^2}{2l_a^2 + 8} = 1 - p,$$

which gives

$$l_a = 2\sqrt{\frac{2p}{1-2p}}. \quad (60)$$

This inductance being substituted in (7) instead of l allows calculation of the voltage response with correct amplitude. Unfortunately, the shape of the voltage response is still not reproduced at this stage.

Improving of consistency of the shape is possible by allowing two fitting parameters, the effective inductance l_s and the amplitude A for the second term of (7):

$$\bar{v}(\phi_e) = w_{J-} - A \frac{l_s^2 w_{J-}^2}{l_s^2 w_{J-}^2 + 4} \left(\frac{i_b}{2} - w_{J-} \right) \tan^2 \phi_e. \quad (61)$$

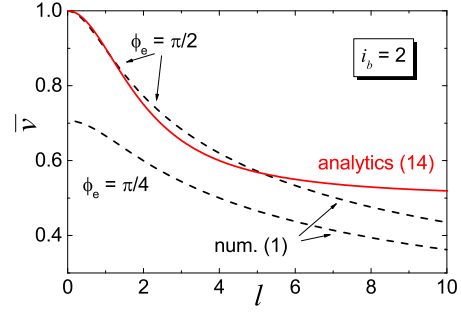


Figure 12. Time-averaged voltage on symmetrical SQUID at $i_b = 2$ calculated using (14) at $\phi_e = \pi/2$ (solid line) and obtained by numerical calculations of (1) at $\phi_e = \pi/2, \pi/4$ (dotted lines).

To define both parameters we introduce another fitting dependence, namely $\bar{v}(l)$ at $i_b = 2$, $\phi_e = \pi/4$ calculated numerically, which is also shown in Fig. 12. This dependence can be approximated by function

$$\bar{v}_{\pi/4}^{num} = \frac{\sqrt{2}}{2} - q, \quad (62)$$

where

$$q = \frac{l^{1.92}}{5.25l^{1.625} + 19.14}. \quad (63)$$

Both fitting parameters l_s, A can be derived from system obtained by equating (61) and (58), (62) at $\phi_e = \pi/2, \pi/4$ correspondingly.

We note that amplitude of the voltage response is found well enough with l_a even for $i_b \neq 2$ that allows introduction of dependence of desired parameters on the bias current. The equation for $\phi_e = \pi/2$ can accordingly be written for arbitrary i_b with the found l_a , and so the system for definition of the desired parameters reduces to

$$A \frac{l_s^2 i_b}{l_s^2 i_b^2 + 16} = \frac{l_a^2 i_b}{l_a^2 i_b^2 + 16}, \quad (64a)$$

$$A \frac{l_s^2}{l_s^2 + 8} \left(1 - \frac{\sqrt{2}}{2} \right) = q. \quad (64b)$$

Solution of the system (64) for l_s, A gives

$$l_s = 4\sqrt{\frac{2(q-p) + pq(i_b^2 - 4) + \sqrt{2}p}{2(i_b^2 p - 2q) - 2pq(i_b^2 - 4) - i_b^2 \sqrt{2}p}}, \quad (65a)$$

$$A = \frac{pq(i_b^2 - 2)}{2(q-p-2pq) + p(\sqrt{2} + i_b^2 q)}. \quad (65b)$$

Frame of validity of this definition corresponds to the range where expression under the square root in (65a) is positive. This range is $l \in [0.35, 6.85]$ for $i_b = 2$ and it increases with increase of the bias current.

Figure 13(a),(b) present comparison of the data obtained by expression (61) (lines) and using numerical calculations of system (1) (dots). It is seen that the

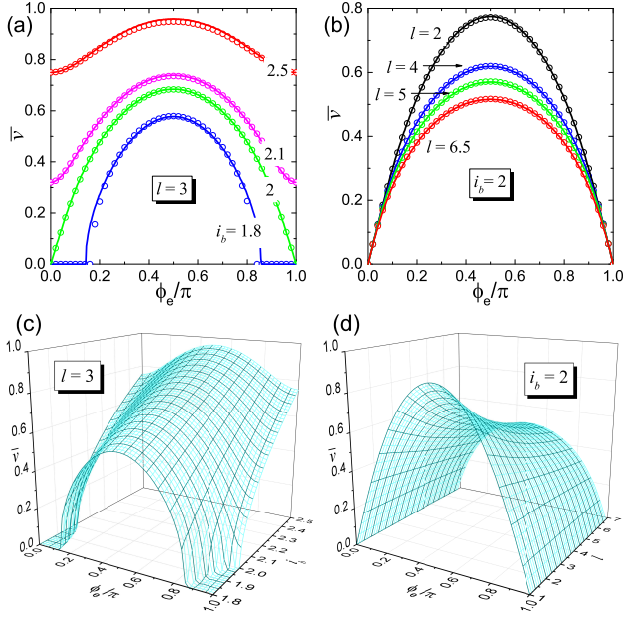


Figure 13. Comparison of SQUID voltage response $\bar{v}(\phi_e)$ obtained using (61) (lines) and using numerical calculations of system (1) (dots) at practical inductance value $l = 3$ for a set of the bias currents $i_b = 1.8, 2, 2.1, 2.5$ (a), and at $i_b = 2$ for a set of the inductance values $l = 2, 4, 5, 6.5$ (b). SQUID voltage response versus i_b at $l = 3$ (c), and versus l at $i_b = 2$ (d) calculated by (61).

data are well consistent especially in the vicinity of the SQUID critical current $i_b \approx 2$. This result allows one to study the voltage response (or IV-curve) as a function of the parameters i_b , ϕ_e , l , and use the data for practical purpose. Corresponding examples of 3D plots are shown in Fig. 13(c),(d).

5.2. SQUID current response

Time-averaged circulating current in symmetrical SQUID can be found similarly using numerical calculations of system (1) and expression (25). Obtained expression for the current response can be rewritten as

$$\bar{i}_{cir}(\phi_e) = A_i \frac{2l_{si}w_{J-}}{l_{si}^2w_{J-}^2 + 4} \left(\frac{i_b}{2} - w_{J-} \right) \tan \phi_e, \quad (66)$$

where l_{si} , A_i are the fitting parameters. While the parameters are defined for arbitrary inductances and bias currents, their expressions are rather complicated

$$A_i = \frac{\left(\frac{i_b}{2}\right)^\beta l^{0.87}}{\left([1 - \alpha]\left(\frac{i_b}{2}\right)^\gamma + \alpha\right)(0.91l^{1.4} + 2.26)}, \quad (67)$$

where

$$\alpha = \frac{l^{2.32}}{1.4l^{2.39} + 0.31},$$

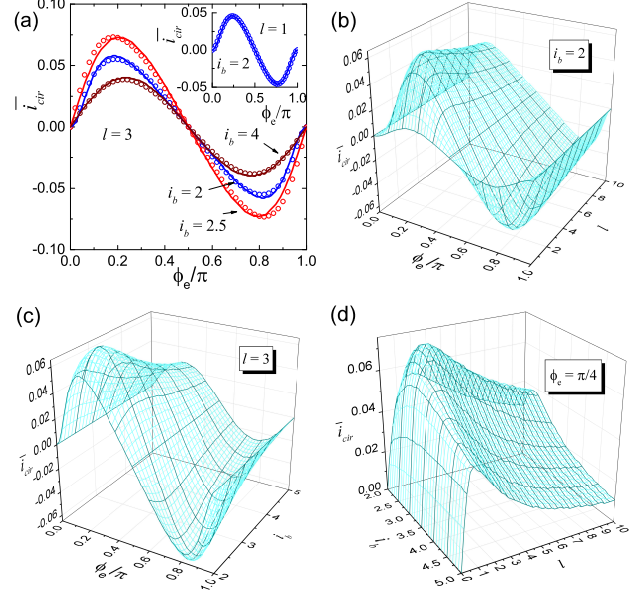


Figure 14. (a) Comparison of SQUID current response $\bar{i}_{cir}(\phi_e)$ obtained by (66) (lines) and using numerical calculations of system (1) (dots) at the inductance value $l = 3$ for a set of the bias currents $i_b = 2, 2.5, 4$. Inset shows curves for $l = 1, i_b = 2$. SQUID current response versus l at $i_b = 2$ (b), and versus i_b at $l = 3$ (c) calculated by (66). (d) The averaged circulating current \bar{i}_{cir} (66) at $\phi_e = \pi/4$ versus the bias current and the inductance.

$$\beta, \gamma = \frac{\sqrt{2} - 1}{f_{\beta, \gamma}} \left(1 + \sqrt{1 - \frac{32f_{\beta, \gamma}^2}{12 - 8\sqrt{2}}} \right),$$

$$f_\beta = \frac{l^{2.97} + 0.69}{6.84l^{3.35} + 6.53}, \quad f_\gamma = \frac{l^{2.84} + 1.15}{6.68l^{3.22} + 9.21},$$

and

$$l_{si} = \frac{\sqrt{2} - 1}{f_l} \left(1 + \text{sgn}(l - 1.3) \sqrt{1 - \frac{32f_l^2}{12 - 8\sqrt{2}}} \right), \quad (68)$$

$$f_l = \frac{l^{2.03} + 1.2}{5.42l^{2.34} + 9.81}.$$

Figure 14(a) shows the time-averaged circulating current calculated at different bias currents and inductances using (66) in comparison with corresponding numerical calculations of system (1). The results indicate that the numerical data are fitted by (66) fairly well.

Dependencies of the SQUID current response versus the inductance and versus the bias current calculated by (66) are presented in Fig. 14(b),(c). It is interesting to note that the time-averaged circulating current has maximum over parameters ϕ_e , l , i_b . Nonzero value of \bar{i}_{cir} means that integral over time of the current circulating in the SQUID in the time interval between switchings of the junctions (when a fluxon is passing by the SQUID) is greater than the one corresponding to leveling of the currents

flowing through the junctions which happens after their switchings.

Obviously, there is no circulating current if the junctions switch simultaneously ($\phi_e = 0$), while if they switch in antiphase ($\phi_e = \pi/2$) the corresponding integrals are equalized. This gives optimum value for ϕ_e maximizing $|\bar{i}_{cir}|$ about $\phi_e = \pi/4$.

The current \bar{i}_{cir} at this applied flux versus both remaining parameters l , i_b are shown in Fig. 14(d). Optimum value for the inductance outflows from the fact that for $l \rightarrow 0$ the junctions are synchronized inphase, and the circulating current is purely symmetric over oscillation period. At the same time, for $l \rightarrow \infty$ the circulating current is negligible due to LR -filtering.

The bias current is taken into consideration through the oscillation frequency w_J . For small bias current the frequency is low, and so the time left after switchings for leveling of the currents flowing through the junctions prevail over the time of fluxon passage, that equalizes impacts of the integrals. High bias currents mean high frequencies w_J at which the circulating current is suppressed by LR -filtering as it was considered in Section 2.

Certain values of the parameters providing maximum time-averaged circulating current can be found from (66) as $\{\phi_e, l, i_b\} = \{0.21/\pi, 2.1, 2.56\}$, at which the current is $\bar{i}_{cir} = 0.076$. The obtained result shows that this current can be safely omitted in symmetrical case in consideration of more complex circuits e.g. a bi-SQUID as it was done in the work [29].

6. Discussion

Results presented in this paper provide qualitative and quantitative understanding of processes involved in formation of DC SQUID voltage and current responses. Obtained expressions of the voltage-flux and current-flux functions for practical values of SQUID inductance can be used in design of SQUID-based circuits.

One of difficult problem is modeling of large SQUID arrays. An array containing 2400 Josephson junctions was utilized in recent work [14] as electrically small antenna capable of detecting radio frequencies from distant sources. While shape of the voltage response is one of the most important characteristics of such structure its numerical calculation is quite time consuming. Indeed standard tools for superconductor circuit simulations as PSCAN practically limit circuit complexity to ~ 500 junctions, so complex schematics have to be broken into several sub-schematics [45]. In this respect the proposed analytical approach to describe SQUID time-averaged characteristics provides valuable solution.

To illustrate the applicability of our approach

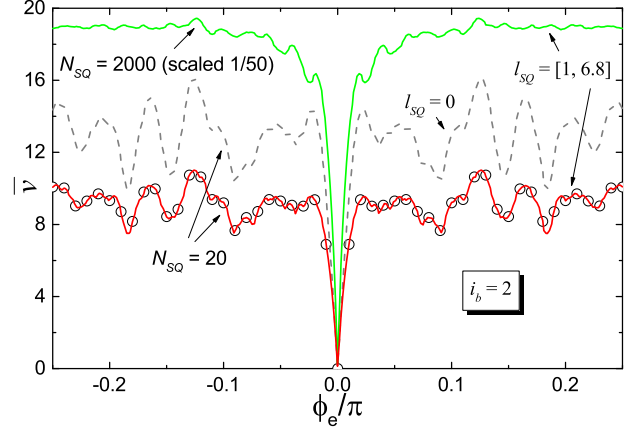


Figure 15. Voltage responses of SQIF structures with normal distribution of inductances of their cells in the range $l_{SQ} \in [1, 6.8]$. Area of the cells are given as $a_{SQ} = l_{SQ}^2$. Curves obtained using presented analytical approach (expression (61)) for SQIF structures with number of cells $N_{SQ} = 20, 2000$ are shown by solid lines (the last curve is scaled 1/50). Dots show data for the SQIF with $N_{SQ} = 20$ calculated numerically using PSCAN. Analytical curve calculated in zero inductance approximation ($l_{SQ} = 0$) for this SQIF with $N_{SQ} = 20$ is presented by dotted line.

to design SQUID arrays we calculate the voltage responses of serial SQIFs with the uniform distribution of inductances of their cells in the range $l_{SQ} \in [1, 6.8]$ at the bias current equal to SQIF's critical current $i_b = 2$, see Fig. 15. It is assumed that area of a cell is proportional to square of its inductance, and so magnetic flux applied to each cell is multiplied by l_{SQ}^2 in our calculations. Curve calculated numerically in PSCAN software tool for SQIF with $N_{SQ} = 20$ SQUID cells is presented by dots. SQIF responses obtained as a sum of cell responses using (61) for the same structure and for SQIF with $N_{SQ} = 2000$ cells are shown by solid lines (the last curve is scaled down 50 times). To display effect of the inductances we calculate the response of the SQIF structure with $N_{SQ} = 20$ putting $l_{SQ} = 0$ and keeping areas of the cells unchanged (dashed line).

It is seen that data calculated numerically and calculated using our analytical approach are perfectly consistent. At the same time, the curve calculated in zero inductance approximation (for $l_{SQ} = 0$) can provide only rough estimation of the voltage response amplitude and shape. We got no significant delay in time of calculation of the curve for the SQIF structure with $N_{SQ} = 2000$ cells compared to the ones with $N_{SQ} = 20$ using our approach. It took about a second on conventional laptop, while corresponding time of numerical calculation would be at least three orders greater. This means that our analytical expressions can be readily used for optimization of such complex circuits.

7. Conclusion

In conclusion, we have developed analytical approach for calculation of DC SQUID voltage and current responses in resistive state for inductance in the range $l \leq 1$. Using two fitting parameters we expanded the frame of validity of our approach to practical values of the inductance up to $l \approx 7$. The circulating current in superconducting state was found for arbitrary values of the inductance. We considered effect provided by technological spread of SQUID parameters relevant for LTS technology generalizing our approach to a case of slightly different critical currents and shunt resistances of SQUID junctions, and unequal SQUID inductive shoulders. We showed that our analytical expressions can be used for calculation of practical SQUID and serial SQUID array responses, confirming this by comparison with numerical calculation results.

Acknowledgments

Authors are grateful to Matthias Schmelz for careful reading of the paper and valuable suggestions. This work was supported by President of Russian Federation grant MK-5813.2016.2, RFBR grants No. 15-32-20362-mol_a_ved, 16-29-09515-ofi_m, Ministry of Education and Science of the Russian Federation, grant No. 14.Y26.31.0007, and grant for leading scientific school No. 8168.2016.2. Mikhail Kupriyanov would like to thank support of Program of Competitive Growth at Kazan Federal University.

Development of analytical description of symmetrical SQUID voltage and current responses was performed under support of RFBR grant No. 15-32-20362-mol_a_ved. Study of effect of small technological spread of parameters on SQUID responses was done in the frame of President of Russian Federation grant MK-5813.2016.2. Applicability of developed analytical expressions to practical LTS SQUID-based circuits design was studied under support of RFBR grant No. 16-29-09515-ofi_m.

References

- [1] Clarke J, Braginsky A I 2004 *The SQUID Handbook* (Weinheim: Wiley) Vol. 1
- [2] Weinstock H (ed) 1996 *SQUID sensors: Fundamentals, Fabrication and Applications* (Dordrecht: Kluwer) pp 1 - 62
- [3] Granata C, Vettoliere A 2016 Nano Superconducting Quantum Interference device: a powerful tool for nanoscale investigations *Phys. Rep.* **614** 1 – 69
- [4] Schönau T, Zakosarenko V, Schmelz M, Stolz R, Anders S, Linzen S, Meyer M, Meyer H-G 2015 A three-axis SQUID-based absolute vector magnetometer *Rev. Sci. Instrum.* **86** 105002
- [5] Chwala A, Stolz R, Schmelz M, Zakosarenko V, Meyer M, Meyer H-G 2015 SQUID Systems for Geophysical Time

- Domain Electromagnetics (TEM) at IPHT Jena *IEICE Trans. Electron.* **E98C** 167 – 173
- [6] Schönau T, Schmelz M, Zakosarenko V, Stolz R, Meyer M, Anders S, Fritzsche L, Meyer H-G 2013 SQUID-based setup for the absolute measurement of the Earth's magnetic field *Supercond. Sci. Technol.* **26** 035013
- [7] Schmelz M, Stolz R, Zakosarenko V, Schönau T, Anders S, Fritzsche L, Mück M, and Meyer H-G 2011 Field-stable SQUID magnetometer with sub-fT Hz^{-1/2} resolution based on sub-micrometer cross-type Josephson tunnel junctions *Supercond. Sci. Technol.* **24** 065009
- [8] Schmelz M, Matsui Y, Stolz R, Zakosarenko V, Schönau T, Anders S, Linzen S, Itozaki H and Meyer H-G 2015 Investigation of all niobium nano-SQUIDs based on sub-micrometer cross-type Josephson junctions *Supercond. Sci. Technol.* **28** 015004
- [9] Prokopenko G V, Mukhanov O A 2013 Wideband microwave low noise amplifiers based on biSQUID SQIFs *International Superconductive Electronics Conference (ISEC), 2013 IEEE 14th ISEC, July 7 - 11*
- [10] Schönau T, Schmelz M, Zakosarenko V, Stolz R, Anders S, Fritzsche L, Meyer H-G 2012 SQIF-based dc SQUID amplifier with intrinsic negative feedback *Supercond. Sci. Technol.* **25** 015005
- [11] Kornev V K, Soloviev I I, Klenov N V, Mukhanov O A 2007 Development of sqif-based output broad band amplifier *IEEE Trans. Appl. Supercond.* **17**(2) 569 – 572
- [12] Zakosarenko V, Schulz M, Krueger A, Heinz E, Anders S, Peiselt K, May T, Kreysa E, Siringo G, Esch W, Starkloff M, Meyer H-G 2011 Time-domain multiplexed SQUID readout of a bolometer camera for APEX *Supercond. Sci. Technol.* **24** 015011
- [13] Kornev V K, Soloviev I I, Sharafiev A V, Klenov N V and Mukhanov O A 2013 Active electrically small antenna based on superconducting quantum array *IEEE Trans. Appl. Supercond.* **23** 1800405
- [14] de Andrade M C, de Escobar A L, Taylor B J, Berggren S, Higa B, Son Dinh, Fagaly R L, Talvacchio J, Nechay B, Przybysz J 2015 Detection of Far-Field Radio-Frequency Signals by Niobium Superconducting Quantum Interference Device Arrays *IEEE Trans. Appl. Supercond.* **25** 1603005
- [15] Kornev V K, Sharafiev A V, Soloviev I I, Kolotinskiy N V, Scripka V A, Mukhanov O A 2014 Superconducting Quantum Arrays *IEEE Trans. Appl. Supercond.* **24** 1800606
- [16] Oppenländer J, Häussler C, and Schopohl N, 2000 Non-Phi(0)-periodic macroscopic quantum interference in one - dimensional parallel Josephson junction arrays with unconventional grating structure *Phys. Rev. B* **63** 024511
- [17] Häussler C, Oppenländer J, and Schopohl N, 2001 Nonperiodic flux to voltage conversion of series arrays of dc superconducting quantum interference devices *J. Appl. Phys.* **89** 1875
- [18] Kornev V K, Soloviev I I, Klenov N V and Mukhanov O A 2009 Bi-SQUID novel linearization method for dc SQUID voltage response *Supercond. Sci. Technol.* **22** 114011
- [19] Kornev V K, Soloviev I I, Klenov N V and Mukhanov O A 2011 Design and Experimental Evaluation of SQIF Arrays With Linear Voltage Response *IEEE Trans. Appl. Supercond.* **21** 394 – 398
- [20] Mukhanov O A, Kirichenko D, Vernik I V, Filippov T V, Kirichenko A, Webber R, Dotsenko V, Talalaevskii A, Tang J C, Sahu A, Shevchenko P, Miller R, Kaplan S B, Sarwana A and Gupta D 2008 Superconductor Digital-RF Receiver Systems *IEICE Trans. Electron.* **E91C** 306 – 317
- [21] Kornev V K, Soloviev I I, Klenov N V and Mukhanov O A 2010 Progress in high-linearity multi-element Josephson structures *Physica C* **470** 886 – 889

- [22] Kornev V K, Soloviev I I, Klenov N V, Sharafiev A V and Mukhanov O A 2011 Linear bi-SQUID arrays for electrically small antennas *IEEE Trans. Appl. Supercond.* **21** 713 – 716
- [23] Longhini P, Berggren A, Palacios A, In V, de Escobar A L 2011 Modeling Non-Locally Coupled DC SQUID Arrays *IEEE Trans. Appl. Supercond.* **21** 391 – 393
- [24] Sharafiev A, Soloviev I, Kornev V, Schmelz M, Stolz R, Zakosarenko V, Anders S and Meyer H-G 2012 Bi-SQUIDS with submicron cross-type Josephson tunnel junctions *Supercond. Sci. Technol.* **25** 045001
- [25] Longhini P, Berggren A, de Escobar A L, Palacios A, Rice S, Taylor B, In V, Mukhanov O A, Prokopenko G, Nisenoff M, Wong E and De Andrade M C 2012 Voltage response of non-uniform arrays of bi-superconductive quantum interference devices *Journ. Appl. Phys.* **111** 093920
- [26] Prokopenko G V, Mukhanov O A, de Escobar A L, Taylor B, de Andrade M C, Berggren S, Longhini P, Palacios A, Nisenoff M and Fagaly R L 2013 DC and RF measurements of serial bi-SQUID arrays *IEEE Trans. Appl. Supercond.* **23** 1400607
- [27] Berggren S, Prokopenko G, Longhini P, Palacios A, Mukhanov O A, de Escobar A L, Taylor B J, de Andrade M C, Nisenoff M, Fagaly R L, Wong T, Cho E, Wong E, In V 2013 Development of 2D bi-SQUID arrays with high linearity *IEEE Trans. Appl. Supercond.* **23** 1400208
- [28] Wu S M, Cybart S A, Anton S M, Dynes R C 2013 Simulation of Series Arrays of Superconducting Quantum Interference Devices *IEEE Trans. Appl. Supercond.* **23** 1600104
- [29] Kornev V K, Sharafiev A V, Soloviev I I and Mukhanov O A 2014 Signal and noise characteristics of bi-SQUID *Supercond. Sci. Technol.* **27** 115009
- [30] Barone A, Paterno G 1982 *Physics and applications of the Josephson effect* (New York: Wiley)
- [31] Likharev K K 1986 *Dynamics of Josephson junctions and circuits* (Amsterdam: Gordon and Breach)
- [32] Chesca B 1998 Analytical theory of DC SQUIDS operating in the presence of thermal fluctuations *J. Low. Temp. Phys.* **112** 165 – 196
- [33] Chesca B 1999 The effect of thermal noise on the IV curves of high inductance dc SQUIDS in the presence of microwave radiation *J. Low. Temp. Phys.* **116** 167 – 186
- [34] Chesca B 1999 The effect of thermal fluctuations on the operation of DC SQUIDS at 77 K – a fundamental analytical approach *IEEE Trans. Appl. Supercond.* **9** 2955 – 2960
- [35] Greenberg Ya S 2002 Theory of the voltagecurrent characteristic of high Tc DC SQUIDS *Physica C* **371** 156 – 172
- [36] Greenberg Ya S 2003 Theory of the voltagecurrent characteristics of high TC asymmetric DC SQUIDS *Physica C* **383** 354 – 364
- [37] Greenberg Ya S, Novikov I L, Schultze V and Meyer H-G 2005 The influence of the second harmonic in the current-phase relation on the voltage-current characteristic of high Tc DC SQUID *Eur. Phys. J. B* **44** 57 – 62
- [38] Groenbech-Jensen N, Thompson D B, Cirillo M, Cosmelli C 2003 Thermal escape from zero-voltage states in hysteretic superconducting interferometers *Phys. Rev. B* **67** 224505
- [39] Romeo F, De Luca R 2004 Effective non-sinusoidal current-phase dependence in conventional d.c. SQUIDS *Phys. Lett. A* **328** 330 – 334
- [40] Torre G, de Luca R 2013 Persistent currents and magnetic susceptibility of two-junction quantum interferometers *Results in Physics* **3** 179 – 181
- [41] De Luca R, Fedullo A and Gasanenko V A 2007 Perturbation analysis of the dynamical behavior of two-junction interferometers *Eur. Phys. J. B* **58** 461 – 467
- [42] Peterson R L and McDonald D G 1983 Voltage and current expressions for a two-junction superconducting interferometer *Journ. Appl. Phys.* **54** 992 – 996
- [43] Jaklevic R C, Lambe J, Silver A H and Mercereau J E 1964 Quantum interference effects in Josephson tunneling *Phys. Rev. Lett.* **12** 159
- [44] Stewart W C 1968 Current-voltage characteristics of Josephson junctions *Appl. Phys. Lett.* **12** 277
- [45] Mukhanov O A 2015 Recent Progress in Digital Superconducting Electronics *International Superconductive Electronics Conference (ISEC), 2015 IEEE 15th ISEC, July 6 - 9*